



Published in final edited form as:

Nat Commun. ; 5: 4072. doi:10.1038/ncomms5072.

## Singlet oxygen Triplet Energy Transfer based imaging technology for mapping protein-protein proximity in intact cells

Tsz-Leung To, Michael J. Fadul, and Xiaokun Shu<sup>1</sup>

Department of Pharmaceutical Chemistry, Cardiovascular Research Institute, University of California, San Francisco, CA 94158

### Abstract

Many cellular processes are carried out by large protein complexes that can span several tens of nanometers. Whereas Forster resonance energy transfer has a detection range of <10 nm, here we report the theoretical development and experimental demonstration of a new fluorescence imaging technology with a detection range of up to several tens of nanometers: singlet oxygen triplet energy transfer. We demonstrate that our method confirms the topology of a large protein complex in intact cells, which spans from the endoplasmic reticulum to the outer mitochondrial membrane and the matrix. This new method is thus suited for mapping protein proximity in large protein complexes.

Protein machines carry out almost every major biological process, including DNA replication, gene transcription, protein translation, and degradation of RNA and protein<sup>1</sup>. Recently, with the use of global proteomic methods, the number of identified stable protein associations has increased<sup>2-4</sup>. To gain insight into molecular mechanisms, Forster resonance energy transfer (FRET) has been widely used to characterize protein-protein interactions<sup>5,6</sup>. FRET is based on the interaction between a donor's emission and an acceptor's absorption dipole moments. Because the dipole-dipole interaction decays rapidly over distance, FRET has a detection range of <10 nm, which limits its application in multi-protein complexes that span several tens of nanometers (nm) in diameter. To overcome FRET's distance limitation, we have developed a new method of molecular imaging: Singlet oxxygen Triplet Energy Transfer (STET).

STET is based on a photosensitizing singlet oxygen generator (SOG) and a fluorescent singlet oxygen sensor (SOS). The proximity of protein X to protein Y can be assayed by fusing X to SOG and Y to SOS. Upon illumination, SOG is excited to the first-excited-singlet-state ( $S_1$ ), which crosses to the first-excited-triplet state ( $T_1$ ) via intersystem crossing (ISC). ISC is made possible through a spin-orbit interaction that flips the spin of the excited

Users may view, print, copy, and download text and data-mine the content in such documents, for the purposes of academic research, subject always to the full Conditions of use:[http://www.nature.com/authors/editorial\\_policies/license.html#terms](http://www.nature.com/authors/editorial_policies/license.html#terms)

<sup>1</sup>To whom correspondence should be addressed. xiaokun.shu@ucsf.edu.

#### AUTHOR CONTRIBUTIONS

X.S. conceived the project. T.-L.T. and X.S. designed the experiments, performed the analyses and wrote the paper. T.-L.T. and M.J.F. performed the experiments.

#### COMPETING FINANCIAL INTERESTS

None declared

electron, resulting in the non-radiative  $S_1 \rightarrow T_1$  transition<sup>7</sup>. The SOG at the  $T_1$  state can then convert triplet oxygen ( $^3O_2$ ) into singlet oxygen ( $^1O_2$ ) through triplet energy transfer<sup>8,9</sup>. Reactive  $^1O_2$  reaching SOS through diffusion reacts with the sensor to alter its fluorescence intensity. Whether or not this reaction is limited by singlet oxygen diffusion depends on the reaction rate of the specific SOS with singlet oxygen. Regardless of this, the fluorescence-intensity change rate of SOS is dependent on the amount of  $^1O_2$  it senses per time (i.e., the flux of  $^1O_2$ ), which is a function of distance: the closer the two proteins are, the faster the fluorescence intensity of SOS changes.

Here, we define the fluorescence-intensity change rate of SOS as STET signal, which reports protein proximity. Because  $^1O_2$  has been estimated to diffuse at least several tens of nm in cells within its half-life<sup>10,11</sup>, STET is expected to function over a greater distance (> 30 nm) than FRET. We use a previously engineered infrared fluorescent protein (IFP1.4) as SOS<sup>12</sup>, and a small singlet oxygen photosensitizer (miniSOG) as a SOG<sup>13</sup>. We first demonstrate that IFP1.4 specifically senses singlet oxygen, but not other reactive oxygen species (ROS), including hydrogen peroxide ( $H_2O_2$ ), superoxide, and hydroxyl radical. We also show that this specific sensitivity of IFP1.4 to singlet oxygen is mainly due to its chromophore, biliverdin (BV). Next, we confirm that singlet oxygen is involved in STET, while other ROS are not. We then demonstrate that STET signal is dependent on the distance between the sensor and the generator, by using linkers of different lengths between SOG and SOS. To demonstrate STET in intact cells, we choose a large protein complex that spans from the ER to the mitochondrial outer membrane and the matrix. We show that STET signal confirms the topology of the complex. Finally, our STET experiment suggests that a mitochondrial inner membrane protein that has previously been shown to genetically interact with other components of the machinery is likely to be part of the complex.

## RESULTS

### Concept of STET

To realize the concept of STET (Figure 1a), we made use of two genetically encoded protein tags, miniSOG and IFP1.4, which require no exogenous cofactors. miniSOG is green fluorescent and generates  $^1O_2$  when illuminated with blue light (450–490 nm)<sup>13</sup>. IFP1.4 absorbs maximally at 684 nm and emits at 710 nm<sup>12</sup>. Thus, there is little spectral overlap between SOG and SOS. Both SOG and SOS are monomeric, making it unlikely for them to alter the stoichiometry of tagged proteins, which is necessary for the correct assembly of complexes.

To demonstrate the dependence of STET on protein proximity, we compared the STET signals of a purified fusion protein of SOG and SOS to that of a mixture of individually purified SOG and SOS. Constant blue light illumination (488 nm) of the fusion protein, which produces  $^1O_2$  from SOG, caused a decrease in the infrared-fluorescence-intensity of SOS (Figure 1b). The natural logarithm of normalized SOS fluorescence-intensity at different time points fits the linear equation  $y = -\alpha t$ , suggesting that SOS senses a constant flux of  $^1O_2$ . In other words, constant illumination of SOG creates a steady-state of concentration gradient of  $^1O_2$ . We calculated the STET signal from the slope ( $\alpha$ ) of the fitted equation (details in **Methods**). Importantly, the SOG/SOS fusion protein has a

significantly larger STET signal than the mixture (Figure 1b), demonstrating that STET reflects protein proximity (see further characterizations in the following sections).

### Reaction of IFP1.4 with reactive oxygen species

To demonstrate that IFP1.4 is a singlet oxygen sensor, we reacted IFP1.4 with various ROS (Figure 2). For the reaction with superoxide, we used two different sources of superoxide: potassium superoxide ( $\text{KO}_2$ ) (Figure 2b); and superoxide generated by the reaction of xanthine oxidase and xanthine (Figure 2c)<sup>14</sup>. Upon addition of superoxide from each source, the fluorescence of IFP1.4 did not change (Figure 2b, c, Methods). On the other hand, the fluorescence of hydrocyanine 3 (a fluorogenic probe for superoxide) increased significantly upon reaction with  $\text{KO}_2$  (Supplementary Figure 1a). Next we reacted IFP1.4 with hydrogen peroxide, which also had no effect on the fluorescence of IFP1.4 (Figure 2d). To test if hydroxyl radical could affect the IFP1.4's fluorescence, we used Fenton's reaction to generate hydroxyl radical by reacting hydrogen peroxide with  $\text{Fe}^{2+}$ . However, the fluorescence of IFP1.4 did not change (Figure 2e). Finally, we reacted IFP1.4 with singlet oxygen. We used two sources of singlet oxygen: 1) reacting hydrogen peroxide with sodium hypochlorite ( $\text{NaClO}$ ) (Figure 2g); 2) Perinaphthenone, an efficient singlet oxygen photosensitizer, which generates singlet oxygen upon blue light excitation (Figure 2h)<sup>15</sup>. IFP1.4 reacted strongly with both sources of singlet oxygen, based on the significant change of its fluorescence (Figure 2g, h). As a control, sodium chlorite has no effect on IFP1.4's fluorescence (Figure 2f). These results demonstrate that IFP1.4 senses singlet oxygen but not other ROS including superoxide, hydrogen peroxide, and hydroxyl radical. We therefore conclude that IFP1.4 is a specific singlet oxygen sensor.

We then tried to explain why IFP1.4 specifically senses singlet oxygen. It is known that ROS including hydrogen peroxide, superoxide, hydroxyl radical and singlet oxygen can generally react with proteins. Our data showing that IFP1.4 only senses singlet oxygen thus suggest that the specificity may come from the chromophore of IFP1.4, biliverdin. To test this hypothesis, we reacted biliverdin with various ROS and monitored its absorbance over time (Figure 3). First, there was no change in the absorbance spectra of biliverdin when we added  $\text{KO}_2$  (Figure 3b), similar to the no-ROS control (Figure 3a). This suggests that biliverdin did not react with superoxide. Similarly, we observed no absorbance change in biliverdin when it was mixed with hydrogen peroxide solution (Figure 3c) or the Fenton's reagent (Figure 3d), suggesting that biliverdin did not react with  $\text{H}_2\text{O}_2$  or hydroxyl radical. Finally, we reacted biliverdin with Perinaphthenone under blue light excitation and detected a significant decrease in the absorbance spectra (Figure 3e), indicating that biliverdin reacted readily with singlet oxygen. Interestingly reaction of biliverdin with singlet oxygen has been previously reported<sup>16</sup>. Our results demonstrate that biliverdin reacts specifically with singlet oxygen but not any other ROS examined here.

Furthermore, reaction of IFP1.4 with singlet oxygen resulted in decrease of the absorbance peak (684 nm) of IFP1.4 (Supplementary Figure 1b). Since the absorbance peak of free BV is 660 nm, and we did not observe blue shift of the IFP1.4's absorbance peak, our data suggests that reaction of IFP1.4 with singlet oxygen does not cause release of bound BV from the protein. Thus the loss of IFP1.4's fluorescence upon reaction with singlet oxygen is

caused by reaction of singlet oxygen with BV. Based on these results, we conclude that the specific sensitivity of IFP1.4 toward singlet oxygen is mainly due to the reaction of its chromophore with singlet oxygen. Although reaction of other ROS with the protein has no apparent effect on the fluorescence of IFP1.4, we cannot exclude the possibility, despite its unlikelihood, that reaction of singlet oxygen with residues in the protein may also contribute to the change of IFP1.4's fluorescence.

### Effect of various ROS quenchers on STET

The demonstration of IFP1.4 as a specific SOS strongly suggests that singlet oxygen is involved in producing the STET signal. To further confirm this, we tried to quench STET using various ROS quenchers (Figure 4). Upon addition of superoxide dismutase (SOD), a superoxide quencher, to the solution of IFP1.4 and miniSOG, we did not observe any effect on STET (Figure 4c, f). The STET signal in the presence of SOD is similar to the control without any quencher (Figure 4b, f). Addition of catalase, a hydrogen peroxide quencher, did not affect STET either (Figure 4d, f). Finally we tested if a singlet oxygen quencher would quench STET. Because sodium azide is known to quench the triplet excited state of flavin mononucleotide (FMN)<sup>17</sup>(the chromophore of miniSOG), we decided to use glutathione (GSH). GSH has been shown to react and quench singlet oxygen efficiently, forming various products including glutathione disulfide, glutathione sulphoxide, glutathione sulphonate, and glutathione sulphinate<sup>18</sup>. Upon addition of GSH, STET is completely quenched (Figure 4e, f) to a level similar to the control without SOG (Figure 4a, f). These results confirm that singlet oxygen is involved in STET, whereas other ROS including superoxide, hydrogen peroxide, and hydroxyl radical are not.

### Dependence of STET on distance

To further demonstrate that STET is dependent on the distance between SOG and SOS, we made three constructs that connect SOG and SOS with linkers of various lengths: 1) 5 amino acids (5aa); 2) 73 aa; and 3) 133 aa. Indeed, the fusion protein of SOG and SOS with the shortest linker produced the largest STET signal, whereas the fusion protein with the longest linker had the smallest STET signal (Figure 5). The fusion protein with the intermediate linker length resulted in an intermediate STET signal. Therefore, our results demonstrate that STET is dependent on the distance between SOG and SOS.

We also examined the dependence of STET on the concentration of SOG. In this case, we mixed different concentrations of SOG with SOS. Upon increasing the concentration of SOG from 0.3  $\mu\text{M}$  to 10  $\mu\text{M}$ , the STET signal increased linearly (Figure 6).

### Demonstration of STET in intact cells

To demonstrate STET in intact cells, we mapped protein proximity within a large protein complex. The ER and mitochondria in *S. cerevisiae* are physically tethered by the ER-mitochondria encounter structure (ERMES)<sup>19</sup>, which spans ~40 nm and is composed of the ER transmembrane protein Mmm1, the two mitochondrial outer membrane (MOM) proteins Mdm34 and Mdm10, and the cytosolic protein Mdm12. In addition, the mitochondrial nucleoid protein Mgm101 co-immunoprecipitates with ERMES<sup>20</sup> and partially co-localizes with Mmm1 by fluorescence<sup>21</sup>. Because replicating mitochondrial DNA (mtDNA) co-

localizes with Mmm1<sup>21,22</sup> (whereas non-replicating mtDNA does not), it has been proposed that mtDNA replication is regulated by the large protein complex that includes ERMES and Mgm101 and spans three membranes from the ER to the mitochondrial matrix<sup>21</sup>. Because ERMES has a known topology across inter-organelle membranes, we elected to use STET to analyze its structure (Figure 7a).

To demonstrate whether STET can map the topology of ERMES, we created three yeast strains that express the following: (i) SOG fused to the cytosolic face of Mmm1 (Mmm1-SOG), and SOS fused to the cytosolic face of Mdm34 (Mdm34-SOS); (ii) Mmm1-SOG, along with SOS fused to Mdm34 facing the intermembrane space (SOS-Mdm34); and (iii) Mmm1-SOG and SOS fused to Mgm101 in the matrix (Mgm101-SOS). Another two yeast strains were created as controls: (iv) Mmm1-SOG and SOS fused to the cytosolic face of the MOM protein Tom70; and (v) Mmm1-SOG and free SOS in the cytosol. Tom70 is part of the translocase of the outer membrane (TOM) complex<sup>23</sup>, and is not associated with Mmm1. We illuminated yeast cells at 488 nm to photo-excite SOG, producing <sup>1</sup>O<sub>2</sub> and green fluorescence; simultaneous illumination at 642 nm was also done to photo-excite SOS. The green (525±25 nm) and infrared fluorescence (705±36 nm) were collected at 100-milliseconds per frame.

First, we observed punctate fluorescent structures in the above strains (Figure 7b–f inset). Similar punctate structures were previously seen with EGFP labeling of the complex, with each punctum representing one junction between ER and mitochondrion<sup>19</sup>. Furthermore, the green fluorescence of Mmm1-SOG:1) overlaps with the infrared fluorescence of SOS fused to Mdm34, consistent with previous results using green and red fluorescent proteins (GFP and RFP, respectively)<sup>21</sup>; and 2) partially overlaps with SOS fluorescence of the Mgm101-SOS, which was observed previously with GFP and RFP labeling<sup>20</sup>. These results indicate that SOG and SOS have no or little effect on assembly of the protein complex.

Secondly, upon blue light excitation of SOG, fluorescence-intensity of SOS decreased in response to <sup>1</sup>O<sub>2</sub> produced by SOG, as: 1) the STET signal of Mdm34-SOS (facing the cytosol) is the greatest (Figure 7b **and** Supplementary Figure 2), 0.082±0.006 per second (s<sup>-1</sup>) averaged from 5 puncta; 2) the STET from Mmm1-SOG to SOS-Mdm34 is smaller (Figure 7c **and** Supplementary Figure 3), 0.052±0.005 s<sup>-1</sup>; 3), and the STET from Mmm1-SOG to Mgm101-SOS is the smallest among the three strains (Figure 7d **and** Supplementary Figure 4), 0.037±0.004 s<sup>-1</sup>. In the strain expressing Mgm101-SOS, STET signal was calculated from the region of fluorescence overlap between Mgm101-SOS and Mmm1-SOG (**Methods**). STET signal in the region of non-overlap is smaller (0.023±0.003 s<sup>-1</sup>), presumably reflecting that SOS in this region is several hundred nanometers away from SOG (their non-overlapping fluorescence suggests larger separation than the light diffraction limit, which is 200 – 300 nm). The differential STET observed in the three strains reflects relative separations between interacting proteins in a cell.

In contrast, the control strains show that STET from Mmm1-SOG to Tom70-SOS is 0.020±0.006 s<sup>-1</sup> (Figure 7e **and** Supplementary Figure 5), while STET from Mmm1-SOG to free cytosolic SOS is 0.017±0.004 s<sup>-1</sup> (Figure 7f **and** Supplementary Figure 6). STET signals in these control strains were calculated from the overlapping region of SOS and SOG

fluorescence. As expected, STET from the non-interacting protein Tom70 is significantly smaller than that of Mgm101 (the overlapping region), despite the fact that both SOG (ER) and SOS (MOM) are on the cytosolic face. In the absence of SOG, there is little change of SOS fluorescence ( $<0.006 \text{ s}^{-1}$ ) under the same illumination conditions (Supplementary Figure 7), suggesting that photobleaching of SOS is negligible. Taken together, the above analysis demonstrates that STET signal confirms the topology of the large protein complex and that STET works over several tens of nanometers (the size of ERMES is  $\sim 40 \text{ nm}$ ), which bridges the imaging gap between FRET ( $< 10 \text{ nm}$ ) and conventional fluorescence microscopy ( $> 200 \text{ nm}$ ).

### Preliminary application of STET

We also used STET to evaluate potential components at the mitochondrial inner membrane (MIM), which connects mtDNA to ERMES. Two transmembrane proteins in the MIM, Mdm31 and Mdm32, were previously shown to be functionally important in maintaining mtDNA<sup>24</sup>. However, it is unknown whether they physically link ERMES to Mgm101 and/or mtDNA. Our preliminary results suggest that the MIM protein Mdm32 could be a physical linker, as evidenced by a strong STET signal of  $0.054 \pm 0.003 \text{ s}^{-1}$  (Figure 8 and Supplementary Figure 8). Nevertheless, further interrogations using genetic and biochemical methods are necessary to confirm our result.

## DISCUSSION

To overcome the distance limitation of FRET, we have developed and demonstrated a new imaging method, STET, based on the long diffusion distance of singlet oxygen over at least several tens of nanometers in cells. Measuring the exact diffusion distance of singlet oxygen in cells is challenging, though. The diffusion distance depends on the singlet oxygen lifetime and the diffusion coefficient of singlet oxygen in the specific part of the cell. It is challenging to measure both values accurately, even though significant advancement has been achieved recently<sup>25</sup>. Although the exact diffusion distance may require further investigation, it seems clear that singlet oxygen can diffuse at least several tens of nanometers in cells within its half-life. Therefore, STET is able to detect protein proximity over much longer distances ( $> 30 \text{ nm}$ ) than FRET ( $< 10 \text{ nm}$ ).

We have demonstrated that IFP1.4 is a specific singlet oxygen sensor by reacting IFP1.4 with different ROS and monitoring its infrared fluorescence. We have further shown that this specificity is due to the specific reactivity of biliverdin, the chromophore of IFP1.4, with singlet oxygen. Although hydrogen peroxide, superoxide, and hydroxyl radical are all known to react with proteins—which would change the local environment of the chromophore—it seems that such a potential change does not perturb the electronic structure of biliverdin in IFP1.4.

We have also verified that singlet oxygen, but not other ROS, is involved in STET by using different ROS quenchers. This is consistent with the original work of miniSOG<sup>13</sup>, in which miniSOG is designed and shown to efficiently polymerize diaminobenzidine (DAB) to generate electron microscopic (EM) contrast in order to locate proteins of interest in cells at

nanometer resolution. It is well known through decades of work that efficient singlet oxygen photosensitizers, such as Eosin, can polymerize DAB<sup>26</sup>.

After the publication of miniSOG, two groups have reported that singlet oxygen generation by miniSOG is complicated. Both groups have observed that initially miniSOG photo-produces singlet oxygen inefficiently, with a quantum yield of  $0.03 \pm 0.01$ <sup>27</sup> or  $0.030 \pm 0.002$ <sup>28</sup>. Under prolonged irradiation, however, the singlet oxygen generation quantum yield increases significantly (up to 10-fold). To explain the initial small singlet oxygen quantum yield of miniSOG, the two groups have proposed different mechanisms though.

On the one hand, Ruiz-Gonzalez et al attributed the small singlet oxygen quantum yield to “a substantial fraction of the nascent <sup>1</sup>O<sub>2</sub> molecules being quenched on their way off the protein”<sup>27</sup>. These authors have proposed that initially, certain residues in the protein quench a significant amount of <sup>1</sup>O<sub>2</sub>, which accounts for the small <sup>1</sup>O<sub>2</sub> quantum yield. After inactivation of those residues, <sup>1</sup>O<sub>2</sub> molecules can efficiently diffuse out of the protein, which explains the irradiation-dependent increase of <sup>1</sup>O<sub>2</sub> quantum yield. On the other hand, Pimenta et al have proposed a different mechanism and hypothesized that type I chemistry is involved, at the expense of singlet oxygen generation by type II chemistry<sup>28</sup>. These authors have proposed that miniSOG photo-generates H<sub>2</sub>O<sub>2</sub> and superoxide ion. The authors are cautious about this hypothesis and have mentioned caveats in their data, though.

Regardless of the disagreement on the possible mechanism for the initially small <sup>1</sup>O<sub>2</sub> quantum yield of miniSOG, both groups agreed and observed that <sup>1</sup>O<sub>2</sub> quantum yield increased significantly over time upon irradiation. As noted by Ruiz-Gonzalez et al, such irradiation-dependent increase of the quantum yield “... may be the reason why miniSOG outperforms other fluorescent proteins reported to date as singlet oxygen generators.” It is also consistent with the previous observations, as mentioned in the miniSOG paper<sup>13</sup>, that miniSOG can polymerize DAB significantly more efficiently than ReAsH (<sup>1</sup>O<sub>2</sub> quantum yield 0.024). It seems to us that under the experimental settings for STET and EM applications, miniSOG photo-generates <sup>1</sup>O<sub>2</sub> efficiently. Interestingly, Pimenta et al observed that even after prolonged irradiation when the <sup>1</sup>O<sub>2</sub> quantum yield increased significantly, photobleaching of miniSOG was not observed, supporting such a notion that miniSOG is “activated” under the EM and STET settings, with no photo-damage during such “activation”.

We have shown that STET is dependent on distance between SOG and SOS. We have further demonstrated that STET is able to confirm the topology of a large protein complex that spans from the ER to the mitochondrial matrix. For future applications of STET in comparing relative proximity between proteins in a protein complex, we suggest fusing SOG to the same protein and fusing SOS to various interacting partners in order to obtain comparable signals. This is because, as we have demonstrated, the STET signal is linearly proportional to SOG concentration. Using the same SOG fusion will more likely assure similar SOG concentration and thus comparable STET signals among different protein pairs. Furthermore, if SOG expression varies among different samples, we suggest to normalize the STET signal by the SOG fluorescence, which is linearly proportional to SOG concentration. We also suggest fixing cells to preserve the protein complex since oxidation



chemically, 1mM of H<sub>2</sub>O<sub>2</sub> and 1mM of NaClO were mixed and added to the IFP or BV solution. To generate <sup>1</sup>O<sub>2</sub> photochemically, 10 μM of perinaphthenone was added to the IFP or BV solution. The reaction mixture was then illuminated with a 450 ± 20 nm blue LED (Innovations in Optics, Woburn MA) at an intensity of ~ 50 mW/cm<sup>2</sup>. The fluorescence emission (for SOS) and absorbance (for BV) spectra were measured at 25°C at different time points. To further demonstrate specificity towards <sup>1</sup>O<sub>2</sub>, STET experiments using a mixture of 1 μM of SOG and 1 μM of SOS in a final volume of 100 μL were performed in the presence of various ROS quenchers (Figure 4). Three ROS quenchers were used: 1U of superoxide dismutase (SOD), 100 mU of catalase, and 1mM of glutathione (GSH). The reaction mixture was illuminated with the 450 ± 20 nm blue LED at ~50 mW/cm<sup>2</sup>. Fluorescence emission spectra of SOS were obtained at different time points. All reactions and spectroscopic measurements were performed in PBS buffer at pH 7.4. The absorbance and fluorescence emission spectra were obtained using the Tecan Infinite<sup>®</sup> M1000 microplate reader. All chemicals were purchased from Sigma-Aldrich, except for xanthine (Calbiochem) and xanthine oxidase (Roche).

### Yeast strains and plasmids

*S. cerevisiae* BY4741 (*Mata his3 1 leu2 0 met15 0 ura3 0*) was used as the parent strain. A heme oxygenase-1 (*HO1*) human gene, flanked by the yeast *TEF1* promoter and *CYC1* terminator, was integrated into the *his3* locus of BY4741 by homologous recombination to generate yTLT027. Heterologous expression of heme oxygenase-1 produces IFP's cofactor, biliverdin. All *S. cerevisiae* strains used in this study were derived from yTLT027. For expression of SOG and SOS fusion proteins, the high-copy episomal vectors p424TEF and p426TEF (from ATCC) were used. Both vectors carry the yeast *TEF1* promoter and *CYC1* terminator. DNA sequences encoding a miniSOG (miniSOG, 0.33kb) and IFP1.4 (0.96kb) were amplified from pcDNA3.1 vectors that carried the mammalian codon-optimized genes. The yeast genes *MDM34* (1.4kb), *MMMI* (1.3 kb), *MDM32* (1.9 kb), *MGM101* (0.8 kb), and the pre-sequence of *TOM70* (first 31 N-terminal residues) were individually PCR-amplified from the genomic DNA isolated from BY4741. An oligonucleotide-mediated recombination method was used to create fusion proteins of miniSOG or IFP1.4 (at the C-terminus) with the above yeast genes directly in yeast cells to give Mmm1-SOG, Mdm34-SOS, Mgm101-SOS, and Tom70-SOS. An additional fusion protein, SOS-Mdm34, was created by fusing IFP to the N-terminus of Mdm34. All fusion proteins were flanked by BamHI and XhoI restriction sites on the vectors. An 8-residue peptide spacer (GDGAGLIN) was inserted between the fusion partners. The nucleotide sequence of the peptide spacer contains a PacI restriction site (ggtgacggtgctggtttaattaac), allowing the swapping of fusion partners. The fusion proteins containing SOG were expressed with p426TEF, whereas those containing SOS were expressed with p424TEF. The constructs used in this study are listed in Supplementary Table 1.

### Yeast growth

Yeast YPD medium containing 1% Bacto-yeast extract, 2% Bacto-peptone, and 2% dextrose was used to grow BY4741 and yTLT027. Synthetic dextrose medium containing 0.67% yeast nitrogen base, 2% dextrose, and amino acid dropout mix lacking tryptophan (for p424TEF selection) and uracil (for p426TEF selection) was used to select for transformants

containing the fusion protein constructs. Yeast cultures were grown at 30° C with constant shaking at 220 rpm. The yeast cells were harvested at the exponential growth phase (OD 0.5–1), fixed with 4% formaldehyde at room temperature for 45 minutes, and washed twice. The cells were then concentrated by centrifugation and attached to the surface of an imaging cover glass coated with Concanavalin A. The edges of the cover glass were sealed with nail polish to prevent drying.

## Imaging

Imaging of purified protein solutions and fixed yeast cells were performed with a Nikon Eclipse Ti inverted microscope with the Perfect Focus System. All instrument control and image acquisition were performed with home-written software in Python. Two diode lasers (488 nm at ~1 W/cm<sup>2</sup> from Stradus, 488-50 and 642 nm at ~3 W/cm<sup>2</sup> from Stradus 642-110; Vortran) were directly shuttered by the computer. A filter wheel was used to control the power of each laser. The two lasers were collimated into a telescopic optical path and focused to the back focal plane of the oil-immersion objective (Olympus 100x UPlanSApo NA 1.4) on the microscope. A quad-band beamsplitter zt405/488/561/640rpc (Chroma) and band-pass filters (ET525/50 for SOG, ET705/72 for SOS, Chroma) were used to separate the fluorescence signal. A two-color split view setup was used to simultaneously acquire SOG and SOS channels within a single image frame. The emitted light was divided by a dichroic mirror (beam splitter 645 DCXR, Chroma), allowing the reflected light path to pass through the ET525/50 for SOG fluorescence and the transmitted light path to pass through the ET705/72 for SOS fluorescence. Both channels were projected on a single camera to produce a split image. The images were recorded with an electron multiplying CCD camera (Ixon DV897DCS-BV, Andor) at a frame rate of 1 Hz (1 second exposure time) for purified protein samples and 10 Hz (100 milliseconds exposure time) for fixed yeast cells.

## Image analysis

The images were analyzed using ImageJ 1.42q (NIH <http://rsbweb.nih.gov/ij/>) and MATLAB (Mathworks). For each acquired image stack, the SOG and SOS channels were extracted from the split-view images and aligned using their corresponding bright-field images. After alignment, we identified candidate Mmm1 puncta from the SOG channel. For each punctum, we defined the corresponding overlapping SOS signal. For each pixel within the overlapping SOS signals, we analyzed the loss in fluorescence over the experiment's time course (typically 5 seconds). The pixel with the highest loss in SOS fluorescence was defined as the center. Drifting, and hence displacement of the center, was uncommon over the time course. As such, pixel-by-pixel alignment was usually not necessary. The signal loss of the immediate neighbor pixels was similar to that of the center (Supplementary Figure 10), rendering pixel-by-pixel calculation of STET signals unnecessary as well. Besides, pixel-by-pixel characterization of STET is subject to large fluctuations in fluorescence intensities. Hence, the signal loss of the center pixel and that of the surrounding 8 pixels (i.e., a 3×3 region) were averaged for each Mmm1 punctum candidate. This average signal loss was used to determine the STET for the punctum. Only puncta with comparable area and SOG fluorescence intensity were analyzed for their corresponding SOS intensity loss. At least five Mmm1 puncta were analyzed per sample.

### Derivation of STET signal

In our system, SOS is irreversibly bleached by singlet oxygen, i.e.,



The mass action kinetics of the above reaction is described as:

$$\frac{d[\text{SOS}_{\text{bleached}}]}{dt} = k[{}^1\text{O}_2][\text{SOS}] \quad (2)$$

The mass balance of SOS is given by:

$$[\text{SOS}_{\text{bleached}}] = [\text{SOS}]_{t=0} - [\text{SOS}] \quad (3)$$

Substitute (3) into (2):

$$-\frac{d[\text{SOS}]}{dt} = k[{}^1\text{O}_2][\text{SOS}] \quad (4)$$

Here,  $[{}^1\text{O}_2]$  is the concentration of singlet oxygen at the site of SOS. In our STET results, the natural logarithm of normalized fluorescence intensity of SOS at different times can be well-fitted by a linear equation:  $y = -\alpha t$ . The first-order kinetics in STET with respect to SOS implies constant singlet oxygen generation over the time course of experiments (i.e.,  $[{}^1\text{O}_2]$  is constant over time). Under such conditions, the solution of (4) is:

$$[\text{SOS}] = [\text{SOS}]_{t=0} e^{-kct} \quad (5)$$

where  $c = [{}^1\text{O}_2]$ . Taking the natural logarithm:

$$\ln \frac{[\text{SOS}]}{[\text{SOS}]_{t=0}} = -kct \quad (6)$$

The STET signal in this study is obtained from fitting the natural logarithm of normalized SOS fluorescence to a linear equation  $y = -\alpha t$ . Comparing this to (6),  $\alpha = kc$ , where  $c$  is governed by diffusion of  ${}^1\text{O}_2$  and is therefore dependent on the distance between SOG and SOS. The quantitative relationship between the STET signal and intermolecular distance should be the subject of future studies.

### Supplementary Material

Refer to Web version on PubMed Central for supplementary material.

## ACKNOWLEDGMENTS

We thank B. Huang, W. Zheng and R. McGorty for assistance in microscopy; P. Walter and C. Osman for yeast strains and constructs; R. Y. Tsien for constructive comments. This work was supported by a NIH Director's New Innovator Award 1DP2GM105446 (to X.S.), a postdoctoral fellowship from the Croucher Foundation of Hong Kong and a NIH T32 training grant (to T.-L. T.).

## REFERENCES

1. Alberts B. The cell as a collection of protein machines: preparing the next generation of molecular biologists. *Cell*. 1998; 92:291–294. [PubMed: 9476889]
2. Havugimana PC, et al. A Census of Human Soluble Protein Complexes. *Cell*. 2012; 150:1068–1081. [PubMed: 22939629]
3. Guruharsha KG, et al. A Protein Complex Network of *Drosophila melanogaster*. *Cell*. 2011; 147:690–703. [PubMed: 22036573]
4. Babu M, et al. Interaction landscape of membrane-protein complexes in *Saccharomyces cerevisiae*. *Nature*. 2012; 489:585–589. [PubMed: 22940862]
5. Fairclough RH, Cantor CR. The use of singlet-singlet energy transfer to study macromolecular assemblies. *Meth Enzymol*. 2009; 48:347–379. [PubMed: 345054]
6. Jares-Erijman EA, Jovin TM. FRET imaging. *Nat Biotechnol*. 2003; 21:1387–1395. [PubMed: 14595367]
7. Tatchen J, Gilka N, Marian CM. Intersystem crossing driven by vibronic spin-orbit coupling: a case study on psoralen. *Phys. Chem. Chem. Phys*. 2007; 9:5209. [PubMed: 19459284]
8. Climent T, González-Luque R, Merchán M, Serrano-Andrés L. Theoretical Insight into the Spectroscopy and Photochemistry of Isoalloxazine, the Flavin Core Ring. *J. Phys. Chem. A*. 2006; 110:13584–13590. [PubMed: 17165886]
9. Schweitzer C, Schmidt R. Physical Mechanisms of Generation and Deactivation of Singlet Oxygen. *Chem Rev*. 2003; 103:1685–1758. [PubMed: 12744692]
10. Hatz S, Lambert JDC, Ogilby PR. Measuring the lifetime of singlet oxygen in a single cell: addressing the issue of cell viability. *Photochem Photobiol Sci*. 2007; 6:1106. [PubMed: 17914485]
11. Baker A, Kanofsky JR. Quenching of singlet oxygen by biomolecules from L1210 leukemia cells. *Photochem Photobiol*. 1992; 55:523–528. [PubMed: 1620729]
12. Shu X, et al. Mammalian expression of infrared fluorescent proteins engineered from a bacterial phytochrome. *Science*. 2009; 324:804–807. [PubMed: 19423828]
13. Shu X, et al. A genetically encoded tag for correlated light and electron microscopy of intact cells, tissues, and organisms. *PLoS Biology*. 2011; 9:e1001041. [PubMed: 21483721]
14. McCord JM, Fridovich I. The reduction of cytochrome c by milk xanthine oxidase. *J Biol Chem*. 1968; 243:5753–5760. [PubMed: 4972775]
15. Oliveros E, et al. Photochemistry of the singlet oxygen [O<sub>2</sub>(<sup>1</sup>g)] sensitizer perinaphthenone (phenalenone) in N,N'-dimethylacetamide and 1,4-dioxane. *New J. Chem*. 1999; 23:85–93.
16. Matheson IB, Toledo MM. The singlet oxygen reactivity of biliverdin. *Photochem Photobiol*. 1977; 25:243–248. [PubMed: 905347]
17. Spikes JD, Shen HR, Kopecková P, Kopecek J. Photodynamic crosslinking of proteins. III. Kinetics of the FMN- and rose bengal-sensitized photooxidation and intermolecular crosslinking of model tyrosine-containing N-(2-hydroxypropyl)methacrylamide copolymers. *Photochem Photobiol*. 1999; 70:130–137. [PubMed: 10461454]
18. Devasagayam T, Sundquist AR, Di Mascio P, Kaiser S, Sies H. Activity of thiols as singlet molecular oxygen quenchers. *J Photochem Photobiol B, Biol*. 1991; 9:105–116.
19. Kornmann B, et al. An ER-mitochondria tethering complex revealed by a synthetic biology screen. *Science*. 2009; 325:477–481. [PubMed: 19556461]
20. Kornmann B, Osman C, Walter P. The conserved GTPase Gem1 regulates endoplasmic reticulum-mitochondria connections. *Proc Natl Acad Sci USA*. 2011; 108:14151–14156. [PubMed: 21825164]

21. Meeusen S, Nunnari J. Evidence for a two membrane-spanning autonomous mitochondrial DNA replisome. *J Cell Biol.* 2003; 163:503–510. [PubMed: 14597773]
22. Youngman MJ, Hobbs AEA, Burgess SM, Srinivasan M, Jensen RE. Mmm2p, a mitochondrial outer membrane protein required for yeast mitochondrial shape and maintenance of mtDNA nucleoids. *J Cell Biol.* 2004; 164:677–688. [PubMed: 14981098]
23. Wu Y, Sha B. Crystal structure of yeast mitochondrial outer membrane translocon member Tom70p. *Nat Struct Mol Biol.* 2006; 13:589–593. [PubMed: 16767096]
24. Dimmer KS, Jakobs S, Vogel F, Altmann K, Westermann B. Mdm31 and Mdm32 are inner membrane proteins required for maintenance of mitochondrial shape and stability of mitochondrial DNA nucleoids in yeast. *J Cell Biol.* 2005; 168:103–115. [PubMed: 15631992]
25. Ogilby PR. Singlet oxygen: there is indeed something new under the sun. *Chem Soc Rev.* 2010; 39:3181. [PubMed: 20571680]
26. Deerinck TJ, et al. Fluorescence photooxidation with eosin: a method for high resolution immunolocalization and in situ hybridization detection for light and electron microscopy. *J Cell Biol.* 1994; 126:901–910. [PubMed: 7519623]
27. Ruiz-González R, et al. Singlet Oxygen Generation by the Genetically Encoded Tag miniSOG. *J Am Chem Soc.* 2013; 135:9564–9567. [PubMed: 23781844]
28. Pimenta FM, Jensen RL, Breitenbach T, Etzerodt M, Ogilby PR. Oxygen-Dependent Photochemistry and Photophysics of ‘MiniSOG,’ a Protein-Encased Flavin. *Photochem Photobiol.* 2013; 89:1116–1126. [PubMed: 23869989]
29. Davies MJ. Singlet oxygen-mediated damage to proteins and its consequences. *Biochem Biophys Res Commun.* 2003; 305:761–770. [PubMed: 12763058]

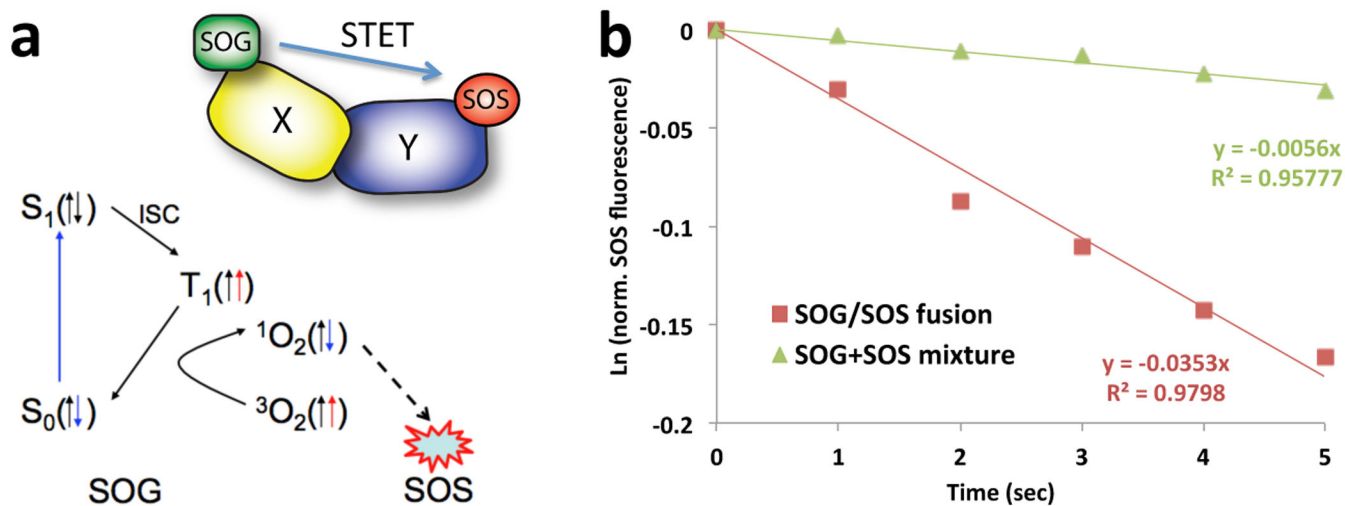


**Figure 1. Development of singlet oxygen triplet energy transfer-based technology**  
**(a)** Schematic diagram showing physical principles of STET. **(b)** Natural logarithm of normalized fluorescence-intensity of SOS over time under blue light illumination in the fusion (1  $\mu\text{M}$ ) versus mixture of SOG and SOS (1  $\mu\text{M}$  each).

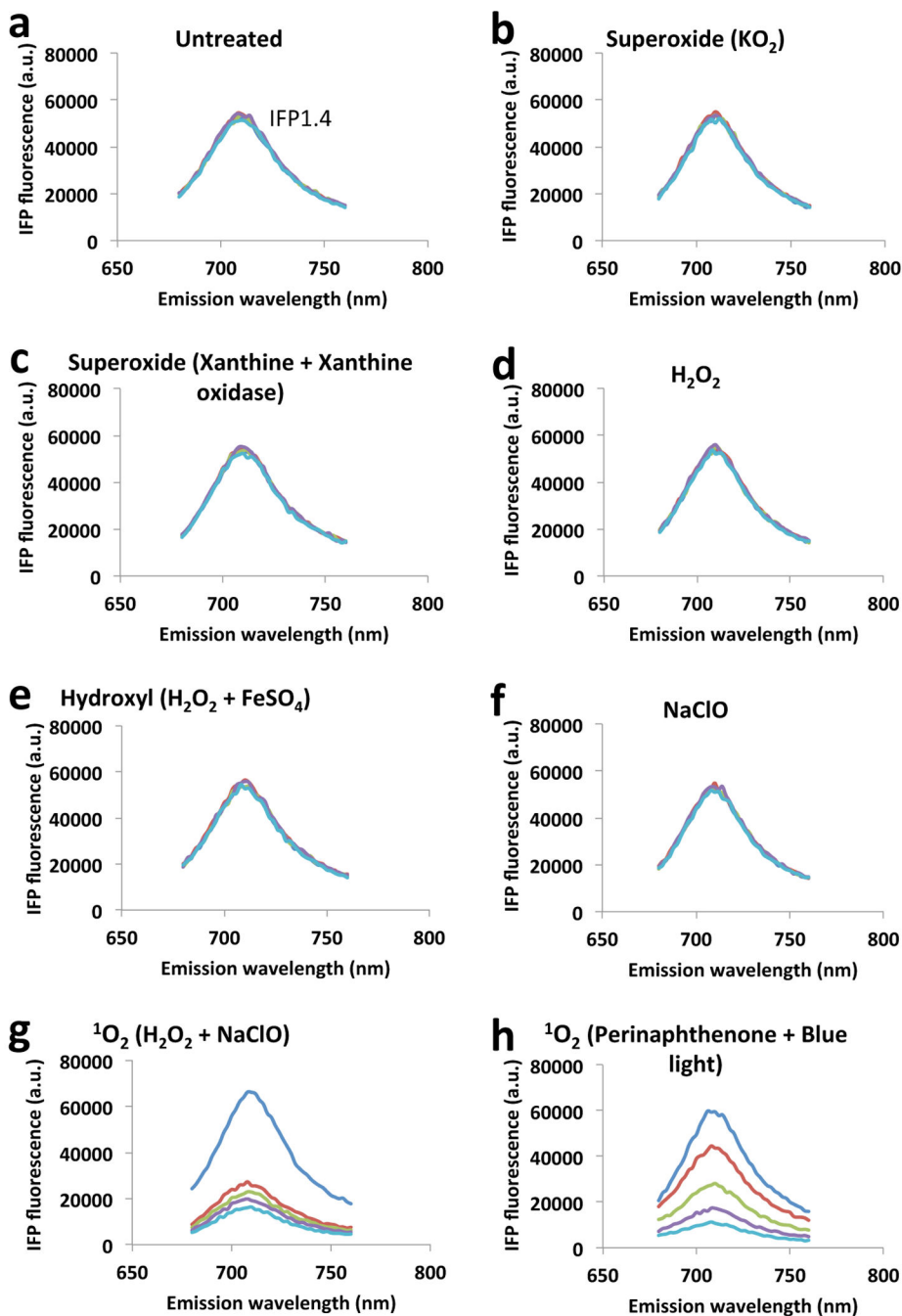


### Figure 2. Reaction of IFP1.4 with reactive oxygen species

Fluorescence spectra of IFP1.4 reacted: (a) without ROS; (b) with superoxide from  $KO_2$ ; (c) with superoxide generated by Xanthine and Xanthine oxidase; (d) with hydrogen peroxide; (e) with hydroxyl radical; (f) with sodium hypochlorite; (g) with singlet oxygen generated from hydrogen peroxide and sodium hypochlorite; and (h) with singlet oxygen photo-generated from Perinaphthenone. Different colors of the lines refer to time after reaction (a – g) or exposure time (h): blue (0 min); red (5 min); green (10 min); purple (15 min); cyan (20 min).

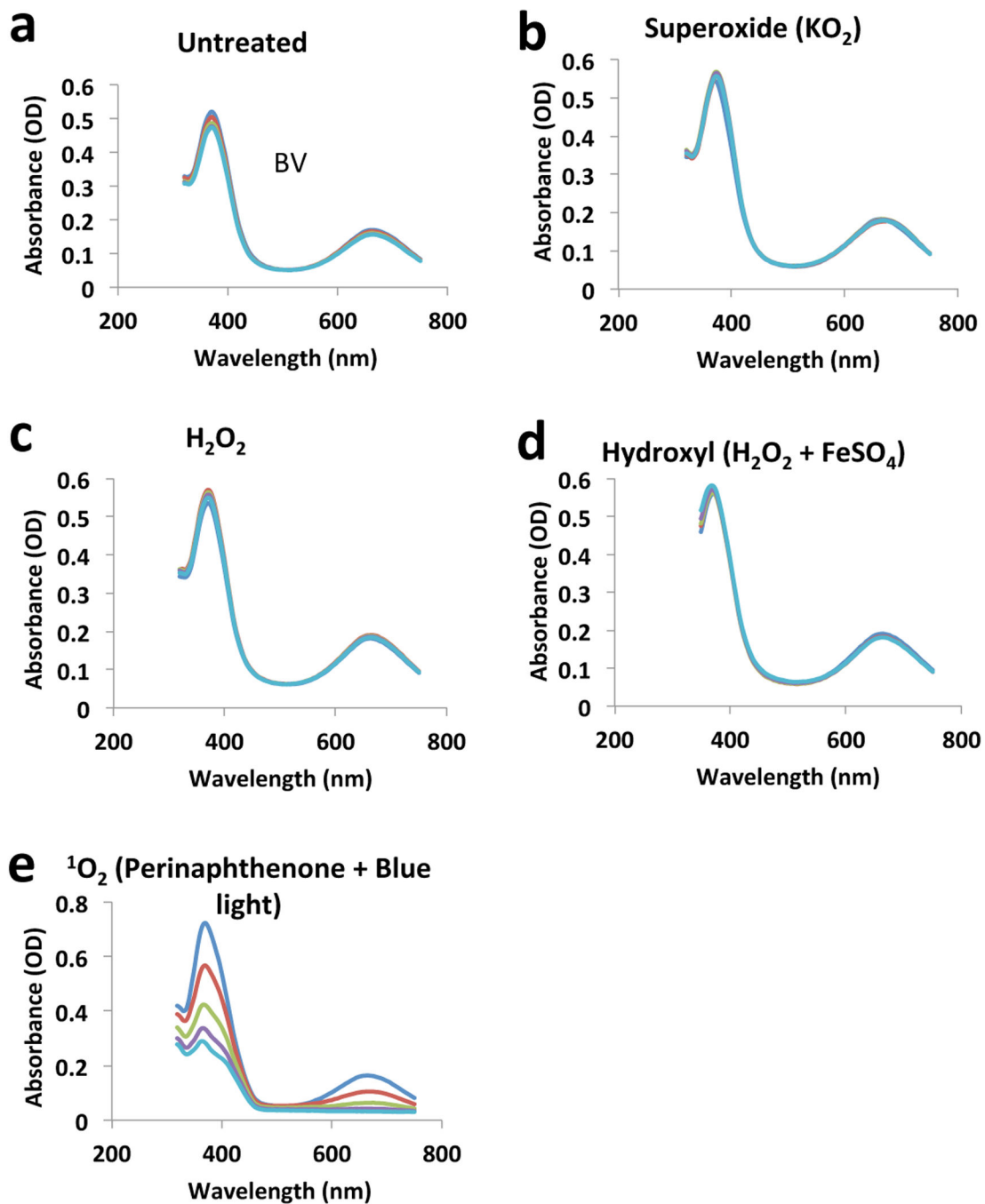


**Figure 3. Reaction of biliverdin with reactive oxygen species**

Absorbance spectra of biliverdin reacted: (a) without ROS; (b) with superoxide from  $\text{KO}_2$ ; (c) with hydrogen peroxide; (d) with hydroxyl radical; and (e) with singlet oxygen photo-generated from Perinaphthenone. Different colors of the lines refer to time after reaction (a – d) or exposure time (e): blue (0 min); red (5 min); green (10 min); purple (15 min); cyan (20 min).

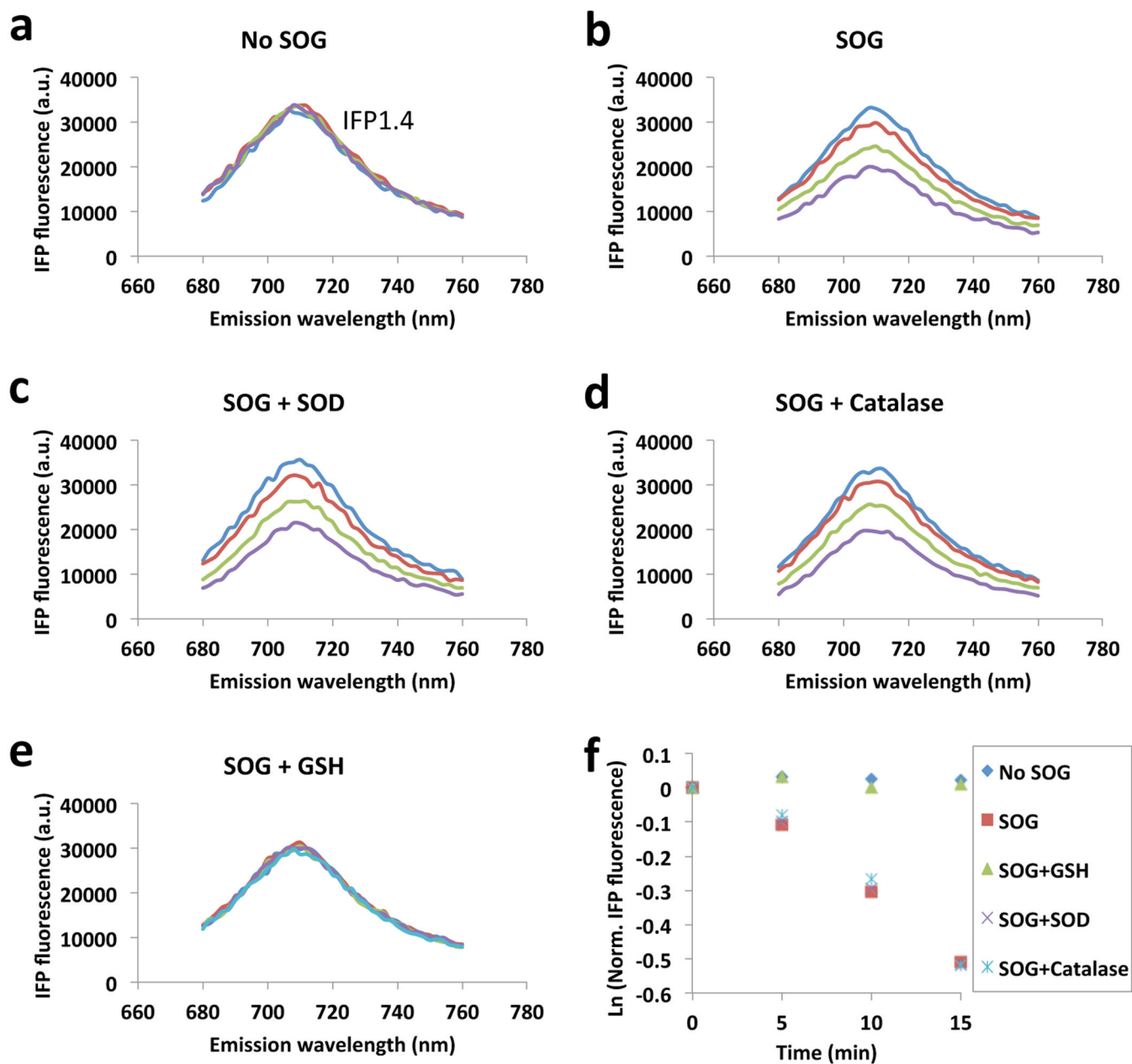


**Figure 4. Quenching of STET with various ROS quenchers**

(a) Fluorescence spectra of IFP1.4 without SOG. (b) Fluorescence spectra of IFP1.4 in the presence of SOG. (c – e) Fluorescence spectra of IFP1.4 in the presence of SOG and (c) superoxide quencher SOD; (d) hydrogen peroxide quencher catalase; and (e) singlet oxygen quencher glutathione (GSH). (f) Natural logarithm of normalized fluorescence-intensity of IFP1.4 over time under blue light illumination. Different colors of the lines refer to time after reaction (a – e): blue (0 min); red (5 min); green (10 min); purple (15 min); cyan (20min, panel e only).

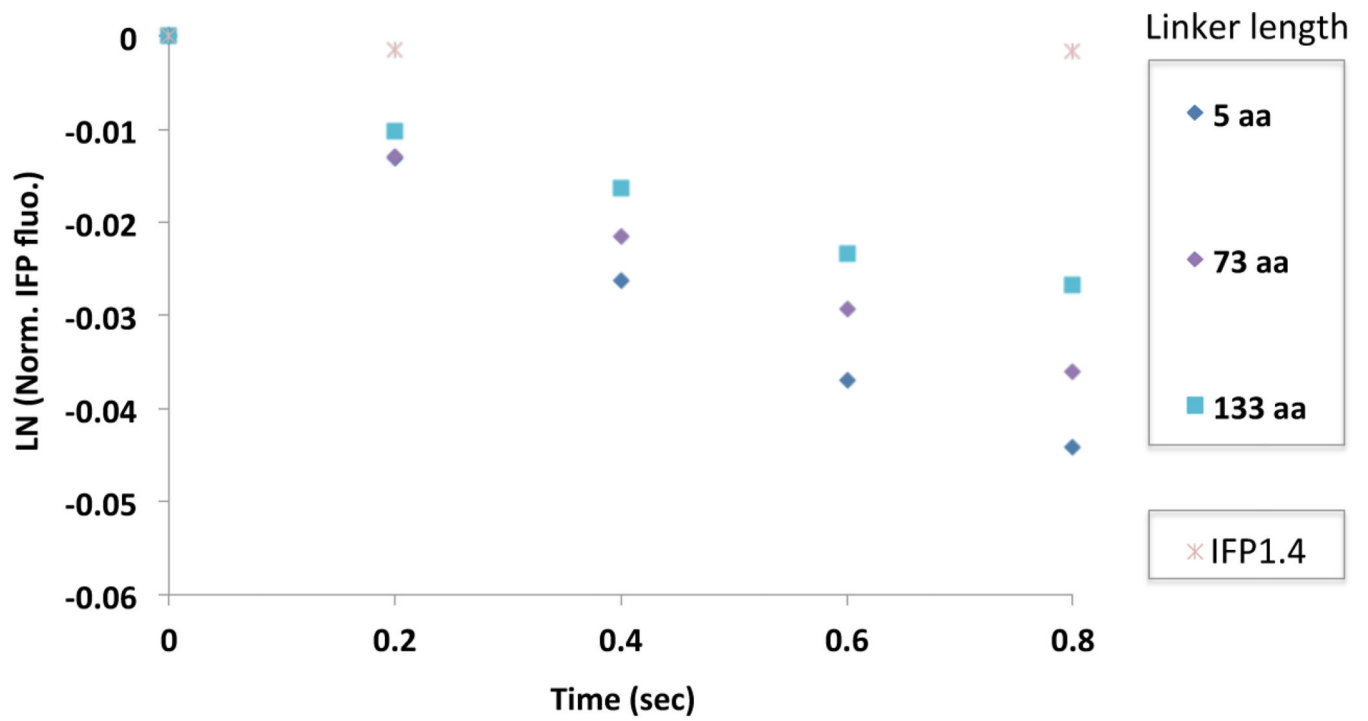


**Figure 5. Dependence of STET on distance between SOG and SOS**  
Natural logarithm of normalized fluorescence-intensity of IFP1.4 over time under blue light illumination.

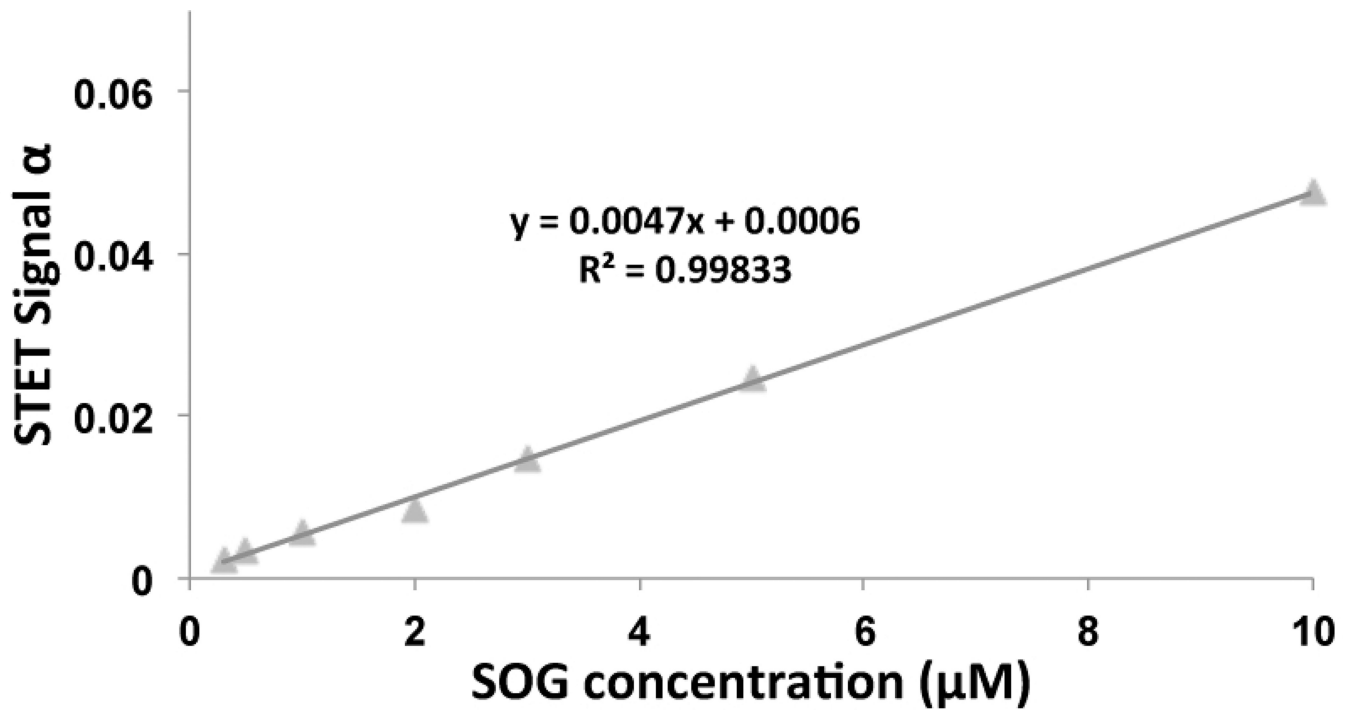


**Figure 6. Dependence of STET on SOG concentration**

The STET signal is obtained from fitting the natural logarithm of normalized SOS fluorescence to a linear equation  $y = -\alpha t$ . The STET signal versus concentration is fitted by a linear line (dashed).

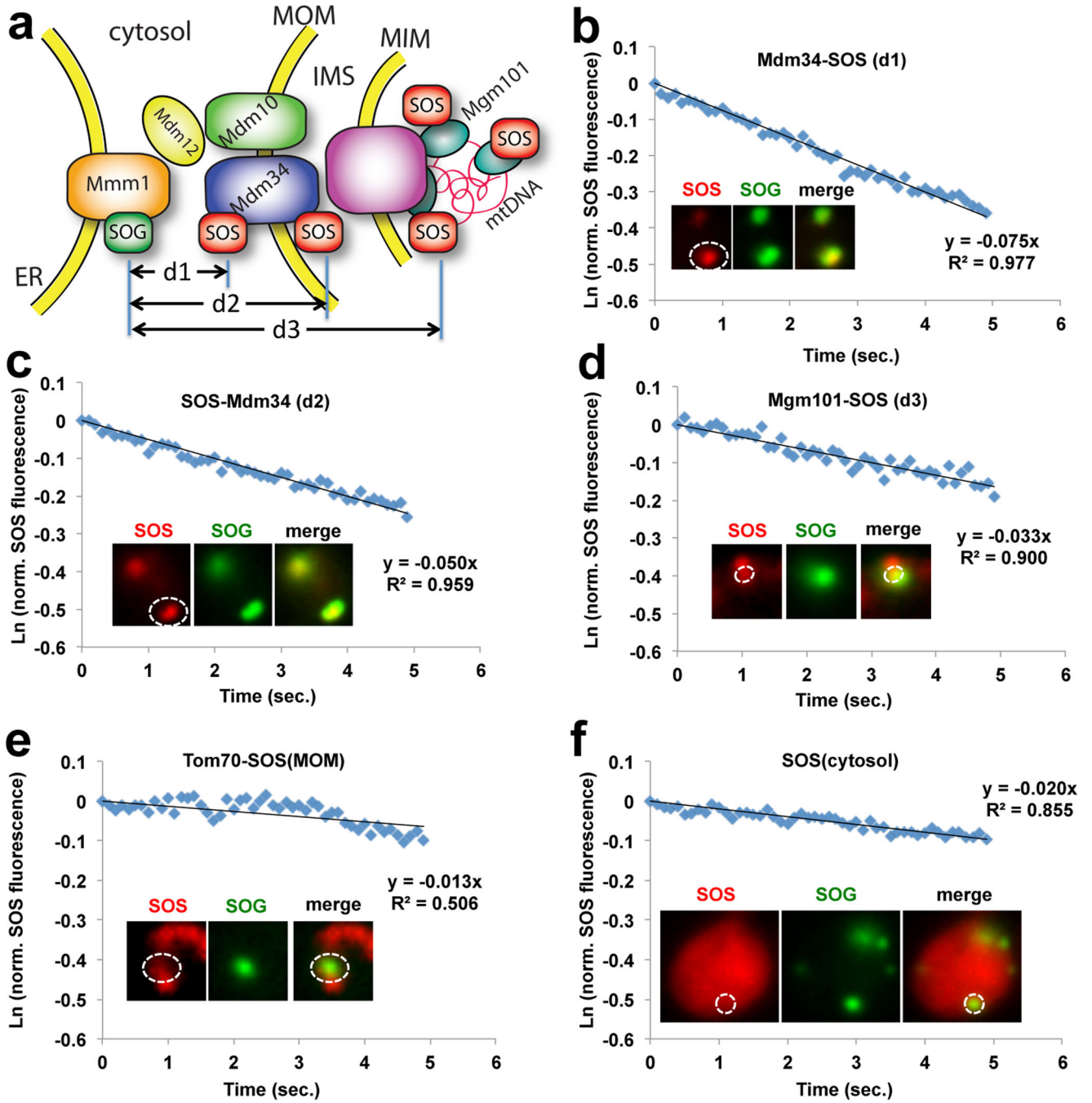


**Figure 7. STET reports protein proximity in intact cells**

(a) Schematic diagram showing topology of the ERMES complex. (b–f) Natural logarithm of normalized fluorescence-intensity of SOS (region within white circle in the inset) over time under blue light illumination (488nm) with SOG attached to the cytosolic face of Mmm1 and SOS to: the cytosolic face of Mdm34 (b); the IMS face of Mdm34 (c); the Mgm101 in the matrix (d); the cytosolic face of Tom70 (e); and the cytosol (i.e., free SOS) (f). IMS: intermembrane space. [MOM: mitochondrial outer membrane. Blue diamond: measured data point. Solid line: linear fit of the data. Insets: fluorescence images at time=0.]

